Electronic Supplementary Material (ESI) for Journal of Materials Chemistry A.

Photosynthesis of Urea from N_2 and CO_2 using Dual Active Sites SiW_6Mo_6@MIL-101(Cr) at Room Temperature

Senda Su, Xiaoman Li *, Wenming Ding, Yue Cao, Shengbo Yuan, Zhenyu Liu, Yang Yang, Yi Ding, and Min Luo*

State Key Laboratory of High-efficiency Utilization of Coal and Green Chemical Engineering, School of Chemistry and Chemical Engineering, Ningxia University, Yinchuan, Ningxia 750021, China

*Corresponding author. Email: lixm2017@nxu.edu.cn, luominjy@nxu.edu.cn

Total number of pages: 28

Total number of figures: 20

Total number of tables: 3

Table of Contents

Experimental section

Materials and general methods

All reagents were used as received without further purification in this work. The chromium nitrate nonahydrate ($Cr(NO_3)_3·9H_2O$, 98%), terephthalic acid (H_2BDC, 99%), sodium bicarbonate ($NaHCO_3$, 99%), sodium molybdate dihydrate ($Na_2MoO_4·2H_2O$, 99%), and N, N-dimethylformamide (DMF, 99.8%) were purchased from Energy Chemical. The silicotungstic acid ($H_4SiW_{12}O_{40}$, 99%), sodium tungstate (Na_2WO_4, 99%), silicomolybdic acid ($H_4SiMo_{12}O_{40}$, 97%), sulfuric acid (H_2SO_4, 98%W), sodium metasilicate nonahydrate ($Na_2SiO_3·9H_2O$, 98%), ethyl ether (CH_3OCH_3, 99%), and hydrochloric acid (HCl, 37%W) were purchased from Aladdin chemistry Co. Deionized water was purified through a Millipore system.

IR spectra were taken on a Perkin-Elmer spectrum One FT-IR spectrometer in the 4000~400 cm^{-1} region with KBr pellets. X-ray diffraction (XRD) data were obtained from an AXS D8 ADVANCE A25 with Cu-Kα radiation (40 kV, 40 mA) of wavelength 0.154 nm (Germany). SEM images were collected from the ZEISS Sigma 300 scanning electron microscope at an accelerating voltage of 30 kV (Germany). TEM images were obtained from a FEI Talos 200S transmission electron microscope operated at 200 kV. XPS measurements were performed on a Thermo Scientific K-Alpha X-ray photoelectron spectrometer using Al as the exciting source. The nitrogen physisorption Brunauer-Emmett-Teller (BET) experiments were collected on a Mike ASAP2460 system. The absorbance data of spectrophotometer were measured on a Persee TU-19 UV-Vis spectrophotometer. The Ion chromatography (IC) was tested on a Thermo Fisher Aquion. Material performance screening by multichannel photochemical reaction system (PCX-50C, Beijing Perfectlight Technology Co., Ltd). In *situ* FT-IR measurements were conducted using the Bruker INVENIO R FT-IR spectrometer equipped with an in situ diffuse reflectance cell (Harrick). The thermogravimetric (TG) was tested on a TGA5500. The gas chromatography (GC) experiments were collected on a GC9790II and were performed in a sealed system. The inductively coupled

plasma-mass spectrometry (ICP-MS) experiments were conducted on the Agilent 7800 (MS).

Electrochemical measurement

The electrochemical measurements were performed on a CHI 660D electrochemical workstation (Shanghai CH Instruments, P. R. China) using a standard three-electrode configuration. A 300W Xe lamp (PLS-SXE300, Beijing Perfect Light Co., Ltd.) was used as light source. For preparing working electrode, catalyst powder was coated on a fluorine-doped tin oxide (FTO) substrate about 2 cm × 2.5 cm square. Firstly, 5 mg of photocatalyst was dispersed in the mixture of 0.49 mL ethanol solution and 10 μL Nafion solution (5 wt%), and the mixtures were ultrasonically scattered for 60 min. Subsequently, 100 μL of above suspension was coated on the FTO glass, after natural evaporation of ethanol and then dry at room temperature for 12 h under vacuum conditions. The catalyst coated FTO substrate was used as the working electrode, Pt plate was as counter electrode, and Ag/AgCl was as the reference electrode. The potentials were converted to RHE scale via calibration with the following equation: *E (vs. NHE) = E (vs. Ag/AgCl) + 0.197*. The electrolyte was 0.1 M Na_2SO_4 solution with bubbling N_2/CO_2 or Ar.

TOCP and carrier lifetime analysis.

The transient open circuit voltage (TOCP) data is obtained by applying external irradiation (PLS-SXE300, Beijing Perfect Light Co., Ltd.) during open-circuit voltage (OCV) test (CHI 660D). The TOCP is equal to the open circuit voltage under light (OCV_{Light}) minus the open circuit voltage without light (OCV_{Dark}), $TOCP = OCV_{Light}$-OCV_{Dark}. The carrier lifetime is calculated from the slope in the TOCP-t decay curve,

$$\tau = -\frac{k_B T}{e}\left(\frac{dOCP}{dt}\right)^{-1}$$

where τ is the carrier lifetime, k_B is the thermal energy of 1.38×10^{-23} J/K and e is the charge power of 1.602×10^{-19} C.

DFT calculation method

Vienna ab initio Simulation Package (VASP) based on the Density Functional Theory

(DFT) was used in all calculations[1, 2]. The Plane-Wave basis sets with an adequate cutoff energy of 400 eV and accurate precision was used. Electron-ion core interactions were represented by the Projected Augmented Wave (PAW) approach [3], while the General Gradient Approximation (GGA) of Perdew, Burke and Ernzerhof [4] (PBE) was used as the exchange-correlational functional to describe the interactions among electrons. The structural data of SiW_6Mo_6 cluster comes from the database (J. Am. Chem. Soc., 2009, 131, 5, 1883). The crystal structure of SiW_6Mo_6 has been pre-relaxed. And the vacuum box around the SiW_6Mo_6 cluster is 26.3 Å × 26.3 Å × 26.3 Å. The Brillouin zone integration was done on a grid of 4 × 4 × 1, with the convergence criterion of 1×10^{-5} eV. The adsorption energies were calculated by using the following equation [5],

$$E_{ads} = E_{total} - E_{sub} - E_{mol}$$

where E_{total} is the total energy of substrates and adsorbate, E_{sub} is the energy of substrates and E_{mol} is the energy of adsorbed molecular.

The free energy of each reduction step was obtained at zero bias potential using,

$$\Delta G = \Delta E + \Delta E_{ZPE} - T\Delta S$$

where ΔE was the reaction energy, ΔE_{ZPE} was the difference in zero-point energies, T was the temperature (298.15K) and ΔS is the reaction entropy[6].

Reference

1. G. Kresse, J. Hafner, Physical Review B, **1993**, 47, 558–561.

2. G. Kresse, J. Furthmuller, Physical Review B, **1996**, 54, 11169–11186.

3. P.E. Blochl, Physical Review B, **1994**, 50, 17953–17979.

4. J.P. Perdew, K. Burke, M. Ernzerhof, Physical Review Letters, **1996**, 77, 3865–3868.

5. Selcuk, S., & Selloni, A. Journal of Physical Chemistry C, **2015**, 119, 9973–9979.

6. Chen, C., Zhu, X., Wen, X. et al. Nature Chemistry, **2020,** 12, 717–724.

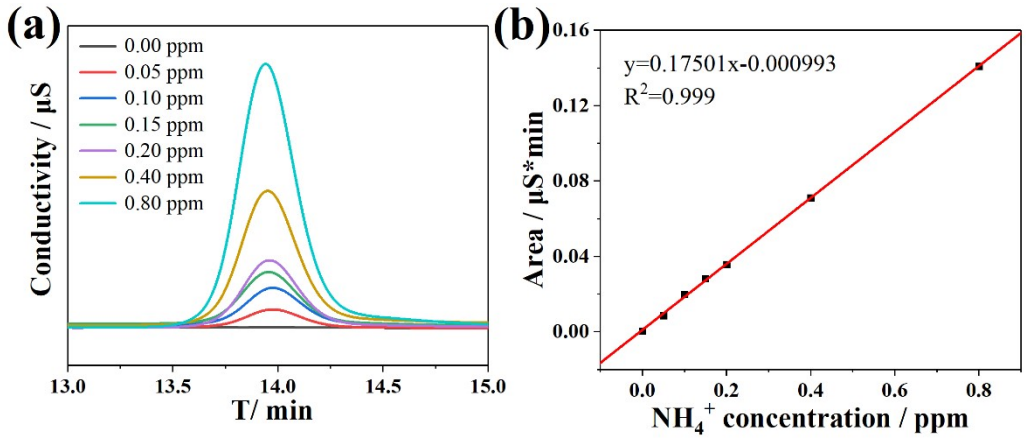

Figure S1. The NH_4^+ detection of standard spectra (a) and fitting curve (b) by ion chromatography.

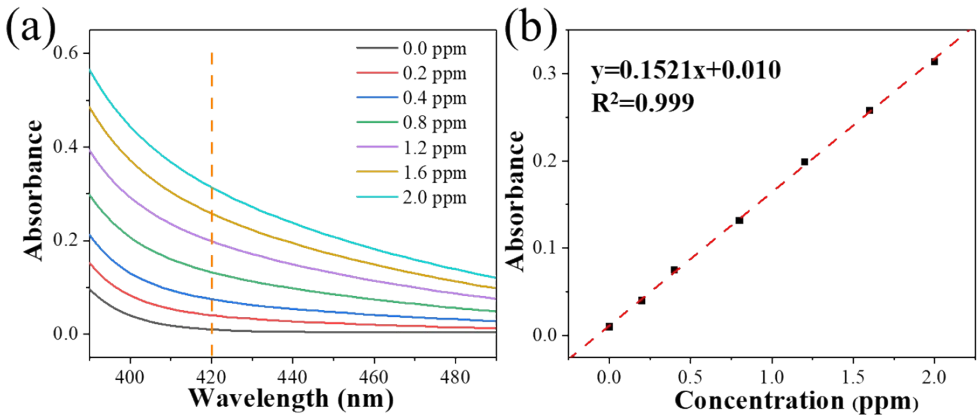

Figure S2. The NH_4^+ detection of UV-vis absorption spectra (a) and fitting curve (b) by Nessler's reagent method.

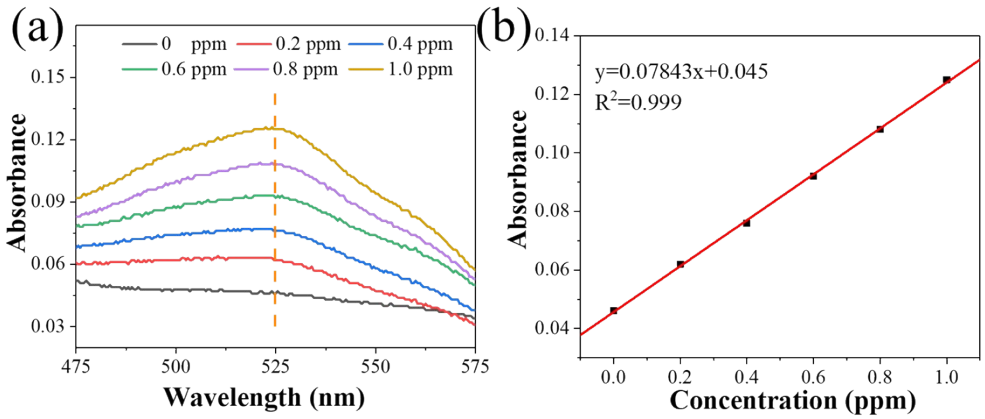

Figure S3. The urea detection of UV-vis absorption spectra (a) and fitting curve (b) by diacetyl monoxime method.

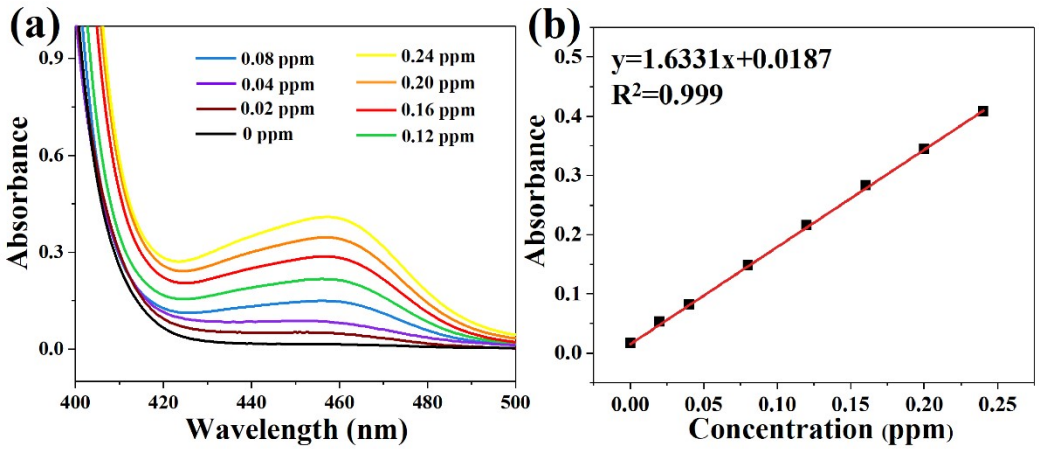

Figure S4. The N_2H_4 detection of UV-vis absorption spectra (a) and fitting curve (b) by Watt-Chrisp method.

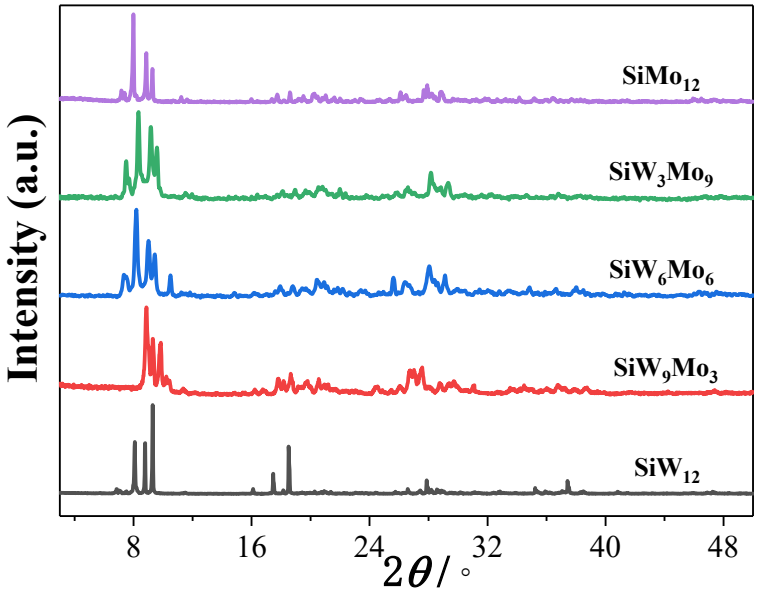

Figure S5. The XRD of $SiW_{12-X}Mo_X$ (X = 0, 3, 6, 9, 12).

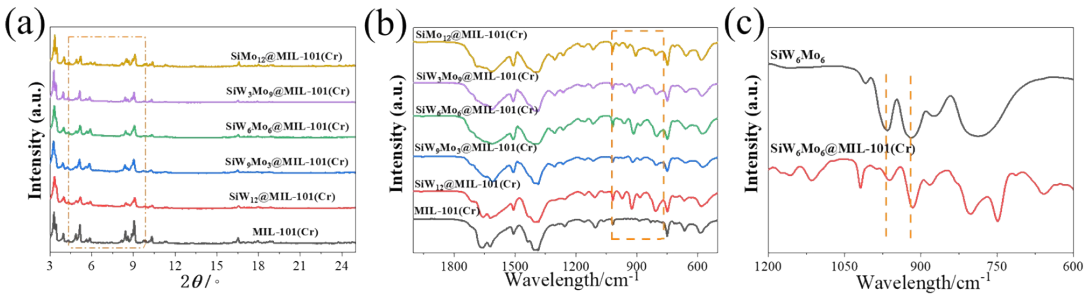

Figure S6. The XRD (a) and FT-IR (b) of MIL-101(Cr) and $SiW_{12-X}Mo_X$@MIL-101(Cr) (X = 0, 3, 6, 9, 12), FT-IR (c) of SiW_6Mo_6 and SiW_6Mo_6@MIL-101(Cr).

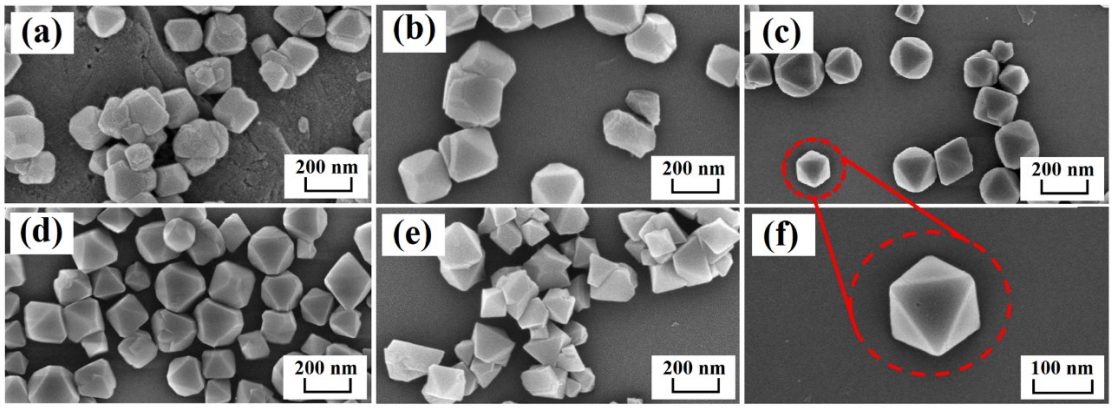

Figure S7. The SEM of SiW_{12}@MIL-101(Cr) (a), SiW_9Mo_3@MIL-101(Cr) (b), SiW_6Mo_6@MIL-101(Cr) (c and f), SiW_3Mo_9@MIL-101(Cr) (d), and $SiMo_{12}$@MIL-101(Cr) (e).

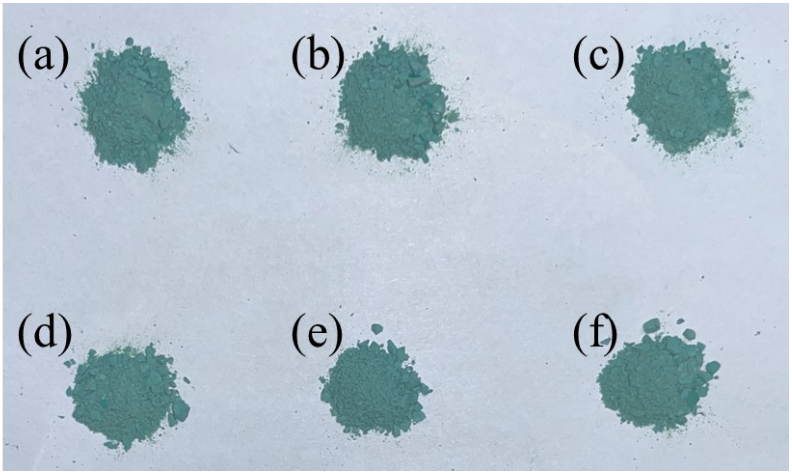

Figure S8. The color photograph of the MIL-101(Cr) (a), SiW_{12}@MIL-101(Cr) (b), SiW_9Mo_3@MIL-101(Cr) (c), SiW_6Mo_6@MIL-101(Cr) (d), SiW_3Mo_9@MIL-101(Cr) (e), and $SiMo_{12}$@MIL-101(Cr) (f).

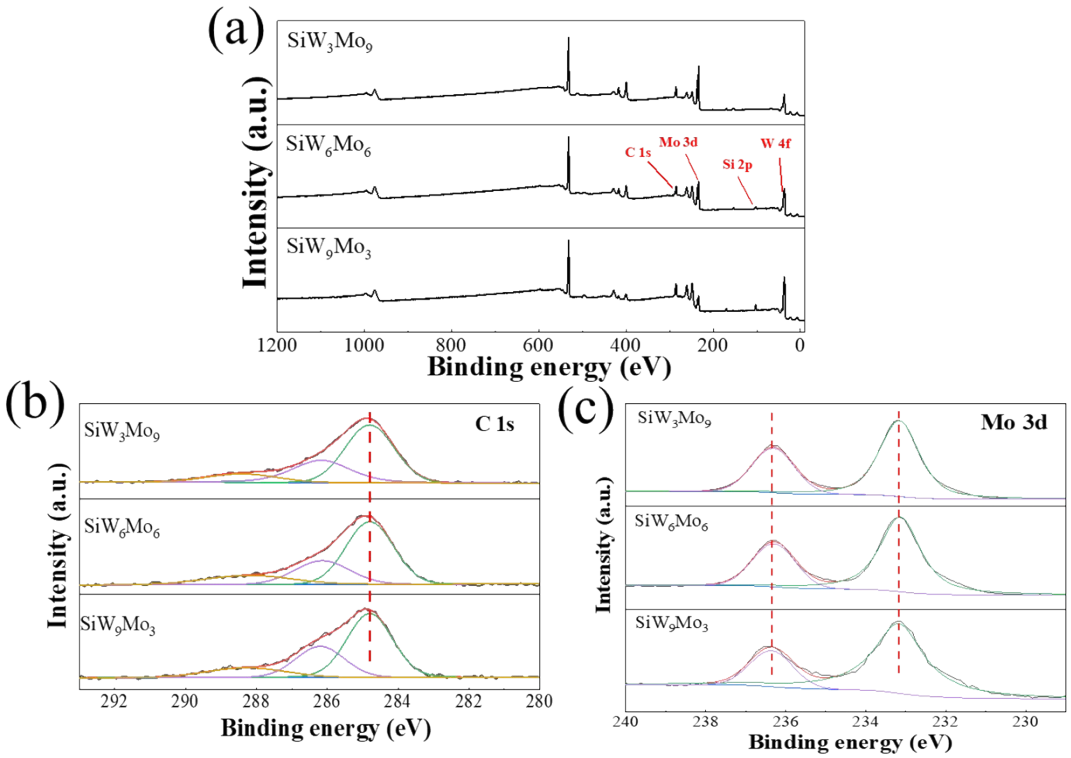

Figure S9. The general (a), C 1s (b), and Mo 3d (c) XPS spectrum of POMs.

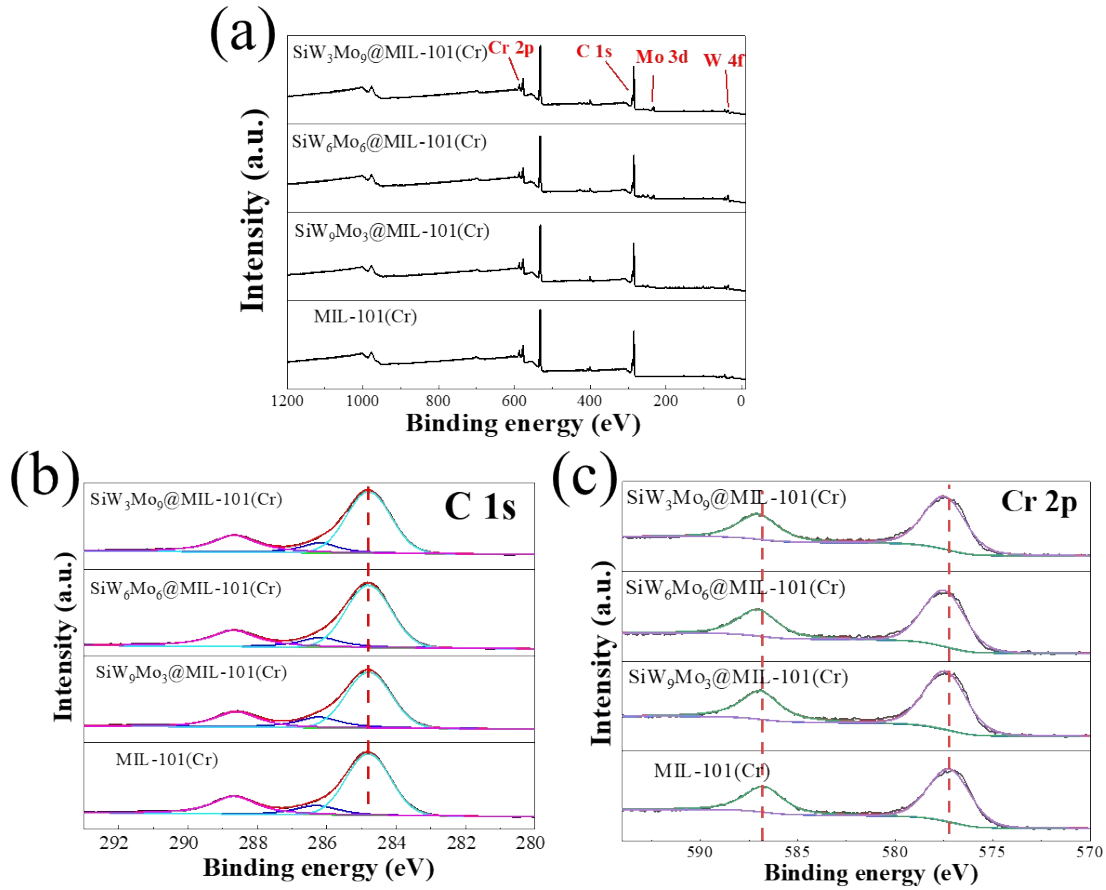

Figure S10. The general (a), C 1s (b), and Cr 2p (c) XPS spectrum of MIL-101(Cr) and $SiW_{12-X}Mo_X$@MIL-101(Cr) (X = 3, 6, 9).

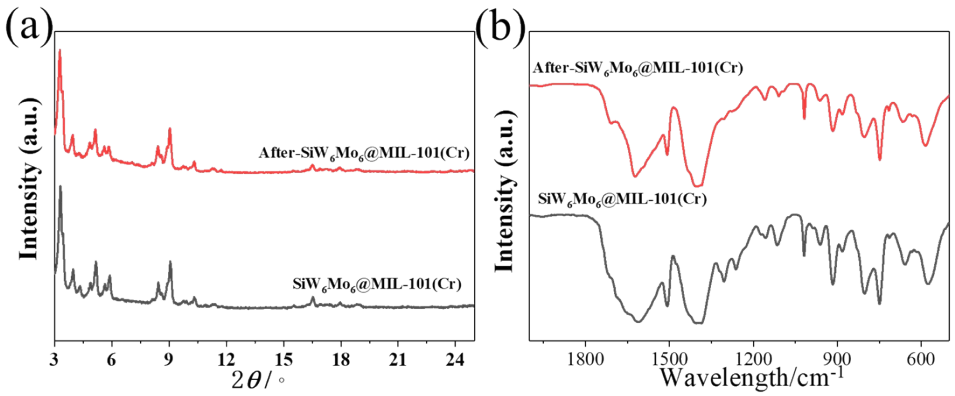

Figure S11. The XRD (a) and FT-IR (b) of SiW_6Mo_6@MIL-101(Cr) before and after cycle reaction.

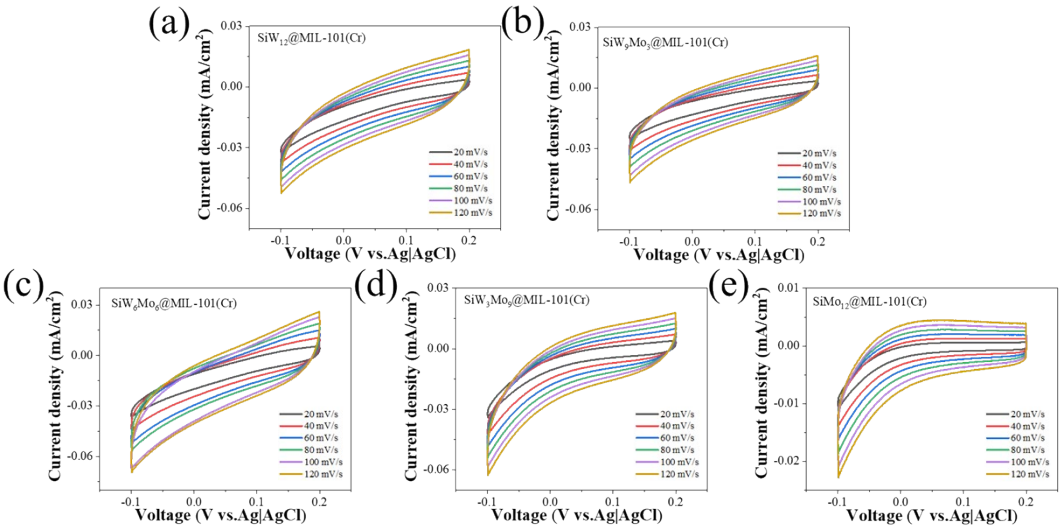

Figure S12. The CV curve of $SiW_{12-X}Mo_X$@MIL-101(Cr) (X = 0, 3, 6, 9, 12).

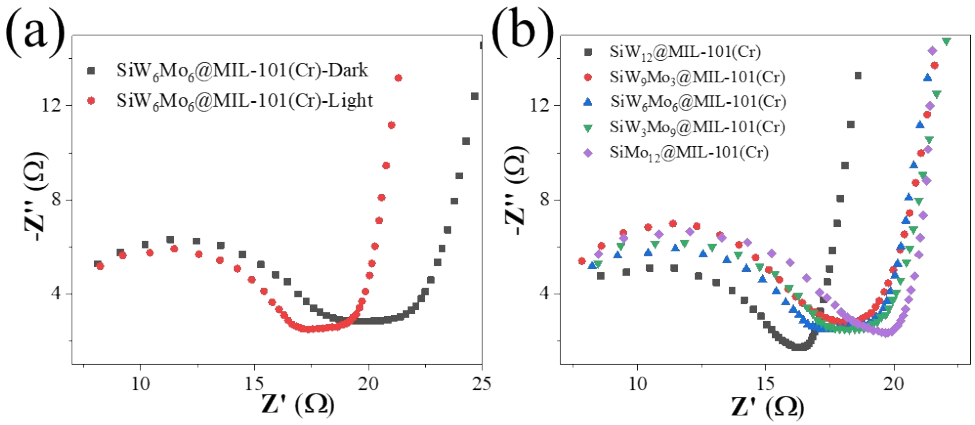

Figure S13. The EIS of $SiW_{12-X}Mo_X$@MIL-101(Cr) (X = 0, 3, 6, 9, 12).

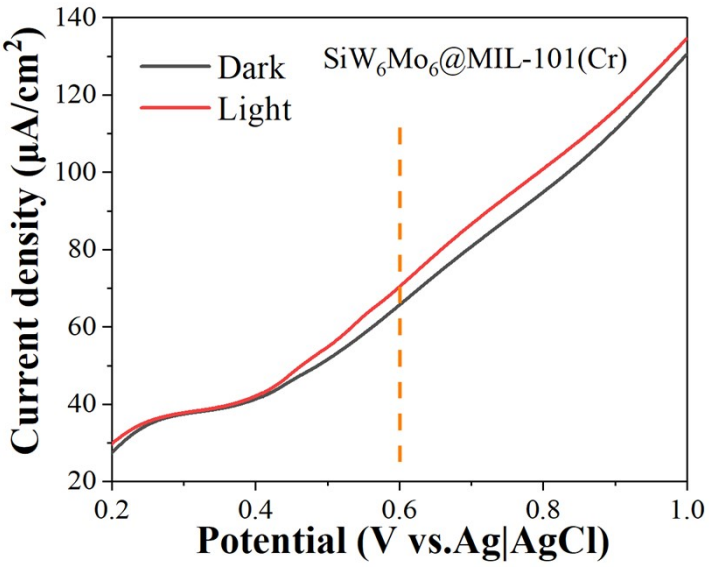

Figure S14. The linear sweep voltammetry (LSV) spectra of SiW_6Mo_6@MIL-101(Cr).

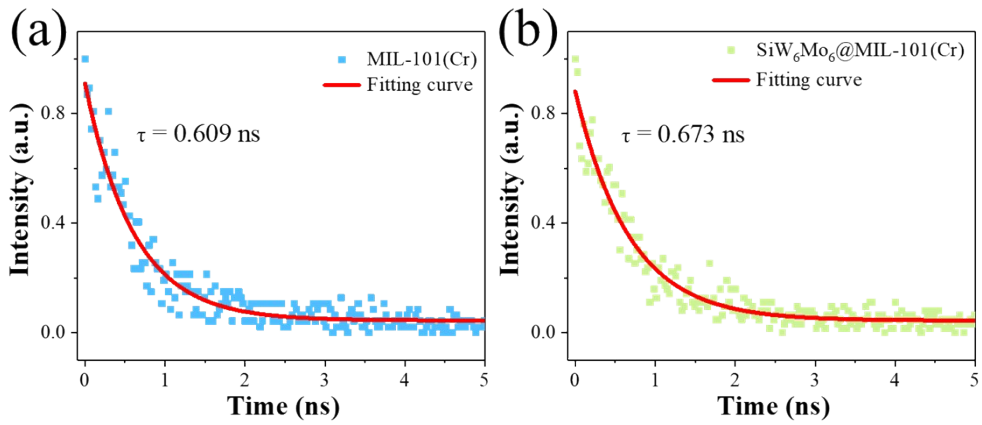

Figure S15. The time-resolved fluorescence decay spectra of MIL-101(Cr) (a) and SiW_6Mo_6@MIL-101(Cr) (b).

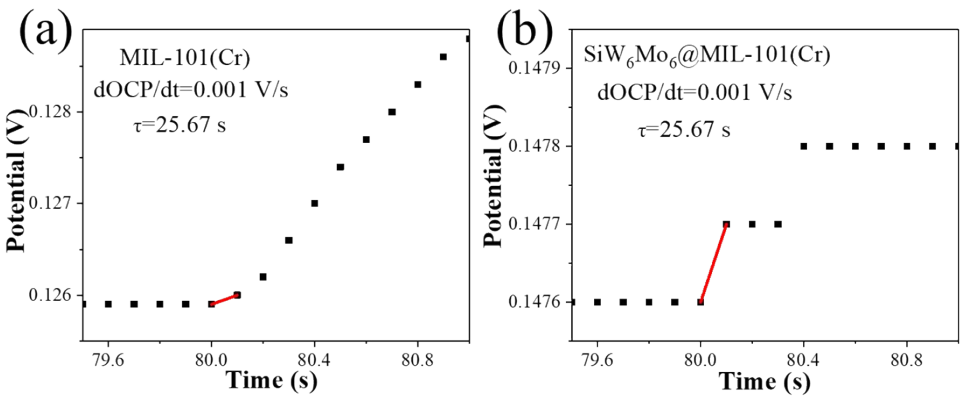

Figure S16. The TOCP of MIL-101(Cr) and SiW_6Mo_6@MIL-101(Cr).

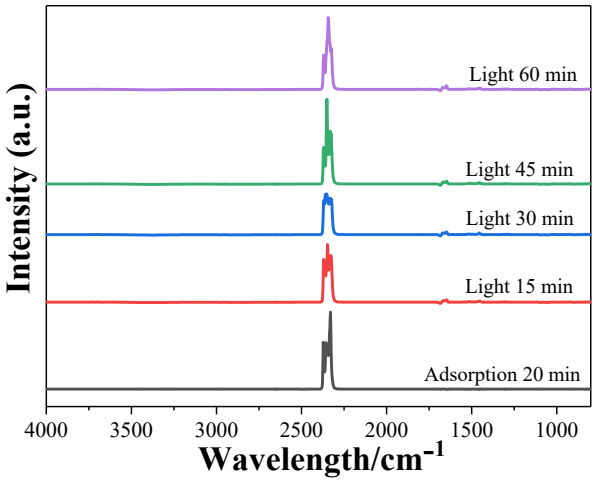

Figure S17. The total *in-situ* DRIFTS of SiW_6Mo_6@MIL-101(Cr).

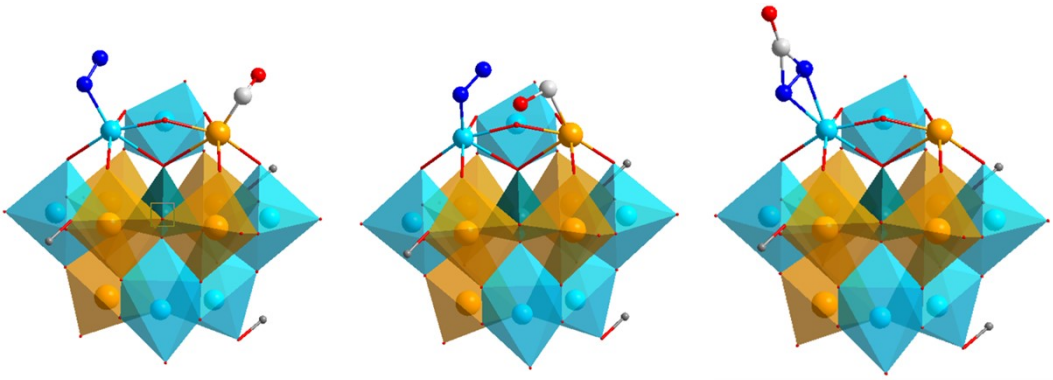

Figure S18. The reaction pathway of *NCON* formation from *CO+*N_2.

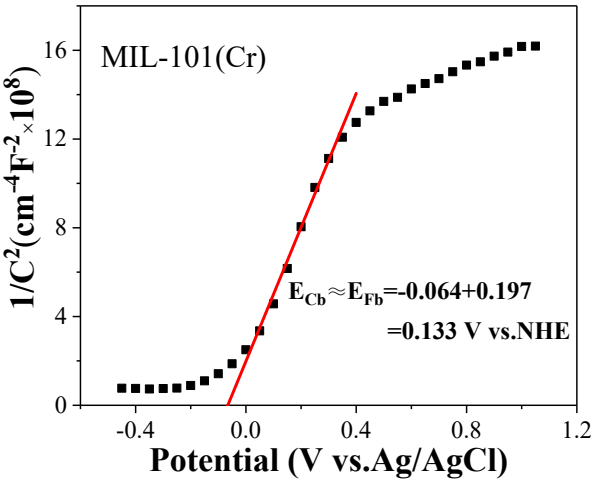

Figure S19. The Mott-Schottky curves of MIL-101(Cr).

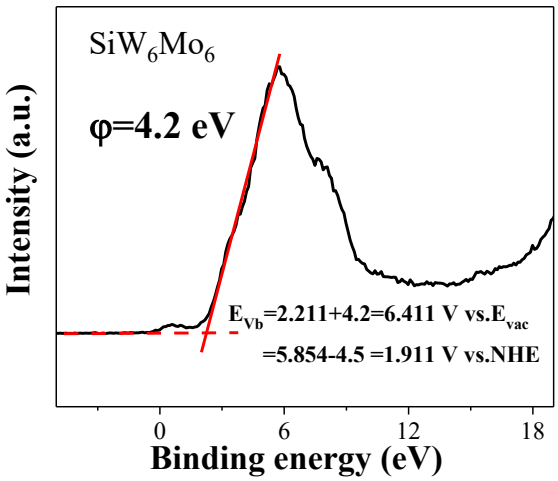

Figure S20. The VB-XPS spectrum of SiW_6Mo_6.

Table S1. The photo/electro-catalytic urea synthesis of different materials.

Catalyst	Reaction type	raw materials	Active site	Urea yield	Reference
V_O-InOOH	electrocatalytic	NO_3^-+CO_2	oxygen vacancies	592.5 $\mu g \cdot h^{-1} \cdot mg^{-1}_{cat}$	1
$In(OH)_3$-S	electrocatalytic	NO_3^-+CO_2	$In(OH)_3$-S	533.1 $\mu g \cdot h^{-1} \cdot mg^{-1}_{cat}$	2
$Ni_3(BO_3)_2$-150	electrocatalytic	NO_3^-+CO_2	Ni	9.70 $mmol \cdot g^{-1} \cdot h^{-1}$	3
Pd_1Cu_1/TiO_2-400	electrocatalytic	N_2+CO_2	PdCu	3.36 $mmol \cdot g^{-1} \cdot h^{-1}$	4
Bi-$BiVO_4$	electrocatalytic	N_2+CO_2	Bi-$BiVO_4$	5.91 $mmol \cdot g^{-1} \cdot h^{-1}$	5
40%2D-CdS@3D-BiOBr	photocatalytic (full spectrum)	N_2+CO_2	undetermined	486 $\mu g \cdot h^{-1} \cdot g^{-1}_{cat}$	6
Cu SA-TiO_2	photocatalytic (at 365 nm)	N_2+CO_2	Cu	432.13 $\mu g \cdot h^{-1} \cdot g^{-1}_{cat}$	7
SiW_6Mo_6@MIL-101(Cr)	photocatalytic (full spectrum)	N_2+CO_2	W (N_2) / Mo (CO_2)	1148 $\mu g \cdot h^{-1} \cdot g^{-1}_{cat}$	This work

1. C. Lv, C. Lee, L. Zhong, et al. Acs Nano, **2022**, 16, 8213-8222.
2. C. Lv, L. Zhong, H. Liu, et al. Nature Sustainability, **2021**, 4, 868-876.
3. M. Yuan, J. Chen, Y. Xu, et al. Energy & Environmental Science, **2021**, 14, 6605-6615.
4. C. Chen, X. Zhu, X. Wen, et al. Nature Chemistry, 2020, 12, 717–724.
5. M. Yuan, J. Chen, Y. Bai, et al. Angewandte Chemie-International Edition, **2021**, 60, 10910-10918.
6. Y. Wang, S. Wang, J. Gan, et al. Acs Sustainable Chemistry & Engineering, **2023**, 11, 1962-1973.
7. D. Li, Y. Zhao, Y. Miao,et al. Advanced Materials, **2022**, 34, 2207793-2207800.

Table S2. The ICP-MS detection data for the solution after 3 h reaction of SiW_6Mo_6@MIL-101(Cr).

detecting element	element concentration
Cr	114.6 μg/L
W	4.4 μg/L

Table S3. Calculated zero-point energies and entropy of different adsorption species.

Species	E_{ZPE} (eV)	TΔS (eV)	G-elect (eV)
CO_2	0.29	0.65	-0.36
H_2	0.28	0.4	-0.12
N_2	0.19	0.15	0.04
NCON	0.35	0.19	0.16
H_2O	0.55	0.67	-0.12
CO+NNH	0.67	0.15	0.52
mid	0.27	0.56	-0.29
COOH+N_2	0.82	0.31	0.51
CO	0.15	0.12	0.03
NCONH	0.69	0.15	0.54
NHCONH	0.98	0.24	0.74
$NCONH_2$	1.02	0.23	0.79
$NHCONH_2$	1.37	0.18	1.19
$NHCONH_2$	1.01	0.98	0.03
$CO(NH_2)_2$	0	0	0
COOH+N_2	0.82	0.31	0.51